Elutriation and agglomerate size distribution in a silica nanoparticle vibro-fluidized bed

Feng, Zhen; Liu, Daoyin; Zhang, Wangle; Feng, Hao; Ruud van Ommen, J.

Important note
To cite this publication, please use the final published version (if applicable).
Please check the document version above.

Elutriation and agglomerate size distribution in a silica nanoparticle vibro-fluidized bed

Zhen Feng [a], Daoyin Liu [a],[*], Wangle Zhang [b], Hao Feng [b], J. Ruud van Ommen [c]

[a] *Key Laboratory of Energy Thermal Conversion and Control of Ministry of Education, School of Energy and Environment, Southeast University, Nanjing 210096, Jiangsu, China*
[b] *State Key Laboratory of Fluorine and Nitrogen Chemicals,168 E. Zhangba Road, Xi'an 710065, Shaanxi, China*
[c] *Department of Chemical Engineering, Delft University of Technology, Van der Maasweg 9, 2629HZ, Delft, The Netherlands*

ABSTRACT

Fluidization of nanoparticle agglomerates is a promising technique to process nanoparticles. However, possible elutriation of small agglomerates may cause significant loss of bed material. To obtain the elutriation behavior under stable operation, in this study the elutriation fraction of silica nanoparticle agglomerates is measured in a vibro-fluidized bed, which is operated for several hours. Among conditions with different fluidizing gas velocities, U_g, and vibration strength, Λ, the lowest elutriation fraction measured is around 5% after 7-hour fluidization. The elutriation fraction increases significantly with U_g, while varies slightly with Λ. To help elucidating the elutriation behavior, the agglomerates at three different locations (bed surface, splash zone, and bed outlet) are sampled and their size distributions are determined. The elutriation rate constant is found to be much smaller than the literature results for ordinary particles, and the reasons are discussed in detail. Finally, an empirical correlation considering size distribution is proposed to fit the elutriation rate constant for the conditions in this study.

1. Introduction

Nanoparticles (particles smaller than 100 nm in at least one dimension) have physical, chemical and mechanical properties that are significantly different from larger particles because of their extreme small size and large specific surface area. Nanoparticles are increasingly used in catalysis [1], medicine [2,3], chemisorption [4] and many other fields. In the fabrication and processing of nanoparticles, a good dispersion of the nanoparticles is required, and fluidization is an efficient technique for dispersing and processing nanoparticle agglomerates.

Nanoparticles are fluidized in the form of porous agglomerates in a range of several tens to several hundreds of micrometers, instead of single primary particles [5]. The fluidization characteristics of nanoparticle agglomerates have been studied extensively [6–14]. The structure of nanoparticle agglomerates during fluidization is well described using the fractal dimension [5,15–18], and quite a few methods for assisting fluidization have been proposed [19–28].

Although nanoparticles can be fluidized, the possibility of elutriation of nanoparticles out of the fluidized beds has been much less studied. For

clarity, the definition of the term elutriation should be distinguished from the entrainment. Entrainment refers to the overall flux of solids carried out of the fluidized bed by gas, while elutriation refers to the selective removal of particles of individual sizes from the fluidized bed [29,30]. For chemical treatment such as atomic layer deposition onto particles in a batch mode, elutriation is undesirable, since it leads to loss of the bed material. Several studies mentioned that elutriation of nanoparticle agglomerates can be reduced by reducing the minimum fluidization gas velocity [17,28,31,32]. In our recent study, Fabre et al. [33] studied entrainment in a nanoparticle fluidized bed and focused on the size distribution of entrained nanoparticle agglomerates above the bed surface. As far as we know, the quantitative values of the elutriation rate of nanoparticle agglomerates in fluidized beds have not been reported so far. For some particle treatments, the process time required is usual several hours. Therefore, it is extremely important to study elutriation of nanoparticle agglomerates during long-time fluidization.

For micron-sized particles, the elutriation of fine powders during fluidization with monodisperse or polydispersity is studied extensively. Wen et al. [29] and Kunii et al. [34] proposed entrainment models in the freeboard of fluidized bed based on the summary of previous

---

* Corresponding author.
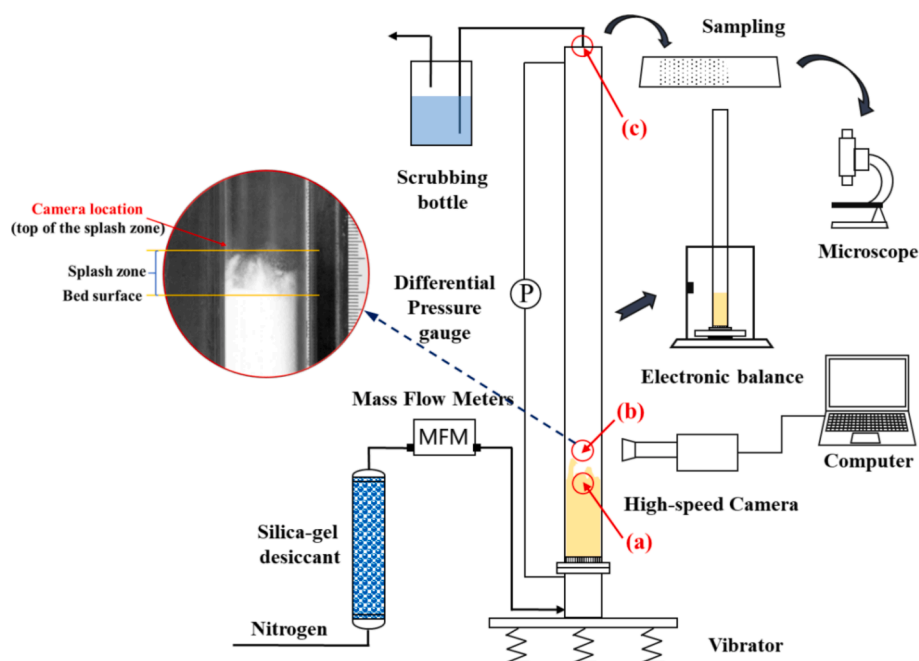 *E-mail address:* dyliu@seu.edu.cn (D. Liu).

Fig. 1. Schematic of the fluidized bed of nanoparticle agglomerates. Sampling locations are noted, (a) bed surface, (b) splash zone, (c) outlet.

Table 1
Experimental conditions.

Condition	Gas velocity (cm/s)	Vibration strength (m/s²)	Sample interval
1	0.75	23.69	
2	1.0	23.69	For each condition: the test lasts for
3	1.25	23.69	420 min, and the interval time is
4	1.0	15.79	30 min.
5	1.0	31.58	

experimental results, and discussed the origin of the ejected particles in the freeboard. Baron et al. [35] found that the smallest particles were not the most easily elutriated from fluidized beds of mixed size particles. Baeyens et al. [36] also found that the elutriation rate constant stabilized with decreasing particle size when the particle size was smaller than the critical size, and proposed an empirical correlation for the elutriation rate constant for group C particles. Afterwards, many researchers have studied the elutriation behavior of group C particles in polydispersity systems [37–44] and found that the elutriation rate constant of group C particles decreased with decrease of particle size when the particle size was smaller than the critical size. Several empirical correlations of the elutriation rate constant applicable to group C particles were proposed and equations for calculating the critical size were given. It should be noted that the predictions by these empirical correlations are significantly different, often by orders of magnitude [30]. Maurer et al. [45] discussed the effect of interparticle and mechanical forces on elutriation, and attributed the significant discrepancy among different correlations to the complexity of the interparticle forces.

This paper aims to quantify and elucidate the elutriation of nanoparticle agglomerates from a fluidized bed. This is different from the case of micron-sized particles, either monodisperse or polydispersity. In nanoparticle agglomerate fluidized beds, the agglomerates are continuously colliding, breaking and recombining during fluidization and form polydisperse clusters. Therefore, with the aim to quantify the elutriation rate of nanoparticle agglomerates at stable operation, the fluidization experiment is performed up to 7 h. The mass of the elutriated nanoparticle agglomerates out of the fluidized bed is measured. The effects of fluidizing gas velocity and vibration strength on elutriation rate is

studied. To help improve understanding the elutriation mechanisms, the agglomerate morphology and size at different positions (bed surface, splash zone, outlet) of the fluidized bed are investigated. Finally, the relationship between elutriation and agglomerate size is discussed.

2. Experimental

2.1. Fluidized bed

The fluidized bed system used in this study is shown schematically in Fig. 1. The column is made of quartz glass with an inner diameter of 24 mm and a height of 450 mm. The gas distributor is made of sintered stainless steel with 20 μm in pore. The fluidizing gas is supplied from a nitrogen cylinder which is dried using silica gel desiccant. The gas flow rate is controlled by a mass flow meter. A differential pressure gauge connected to the bottom and the outlet of the fluidized bed is used to measure the bed pressure drop. A scrubbing bottle is connected to the outlet to prevent contamination by the elutriated particles. The fluidized bed column is mounted on a vibrator, which can generate vertical mechanical vibration. The inner and outer walls of the fluidized bed are coated with an electrostatic eliminator to exclude the effects of electric adhesion. The mass of the elutriated agglomerates is determined by measuring the mass of the entire fluidized bed before and after fluidization test using an electronic balance, whose resolution is 0.001 g. Three locations of sampling the agglomerates are also noted in Fig. 1, that (a) the bed surface, (b) the splash zone, (c) the bed outlet. The details of the sampling and measurement of agglomerates are described in Section 3.2.

2.2. Material and test conditions

The bed material is silica nanopowder, named as PST-S02 supplied by Paukert, Nanjing. The primary particle has a size of 20 nm, material density of 2200 kg/m³, bulk density of 150 kg/m³, specific surface area of 150 m²/g, and hydrophobic surface. Before each test, the large agglomerates formed during storage are removed by a sieve with pore size of 225 μm, then the particles are dried at a temperature of 130 °C for 3 h to remove moisture.

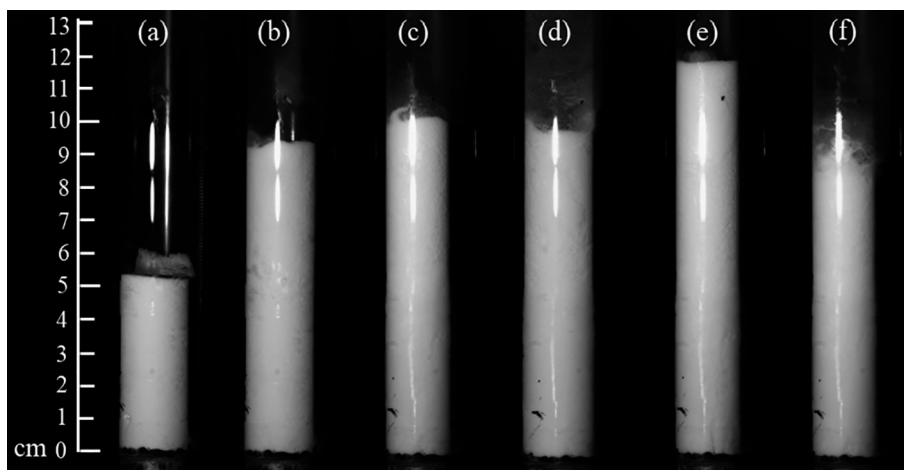The experiments are carried out at room temperature and atmo-

Fig. 2. Images of fluidization with assistance of vibration at different fluidizing gas velocities, (a) initial bed height, (b) $U_g = 0.75$ cm/s, $\Lambda = 23.69$ m/s^2, (c) $U_g = 1.0$ cm/s, $\Lambda = 23.69$ m/s^2, (d) $U_g = 1.25$ cm/s, $\Lambda = 23.69$ m/s^2, (e) $U_g = 1.0$ cm/s, $\Lambda = 15.79$ m/s^2, (f) $U_g = 1.0$ cm/s, $\Lambda = 31.58$ m/s^2.

spheric pressure. Experiments are conducted using 3 g of SiO$_2$ nanoparticles, with an initial bed height of 50 mm. In order to quantify the elutriation rate under sufficiently stable states, each test is lasted for 7 h. The fluidizing gas velocity and vibration strength are changed to study their effects on the elutriation behavior, whose values are listed in Table 1. The vibration strength is expressed in terms of effective vibration acceleration shown below.

$$\Lambda = A(2\pi f)^2 \tag{1}$$

where Λ is the vibration strength (m/s^2), A the amplitude (m), and f the vibration frequency (Hz). In this work, A is chosen as 1.0 mm, 1.5 mm, or 2.0 mm, while f is fixed at 20 Hz, based on our previous study [19]. The fluidizing gas velocity is selected based on the minimum fluidization velocity (U_{mf}) of the nanoparticle agglomerates. The U_{mf} is around 0.9 cm/s without vibration assistance. As the vibration strength increases, U_{mf} first decreases to around 0.6 cm/s, then increases slightly to around 0.7 cm/s and remains stable. At the vibration strength used in this work, U_{mf} is approximately between 0.6 cm/s and 0.7 cm/s. Detailed results of U_{mf} can be found in our previous article [19].

3. Analysis methods

3.1. Elutriation behavior

In order to express the magnitude of the elutriation rate, an elutriation fraction is defined as follows:

$$R_e(t) = \frac{W^e_{tot}(t)}{W_0} \tag{2}$$

where $W^e_{tot}(t)$ represents the total mass of the elutriated bed material out of the fluidized bed at time t and W_0 is the initial mass of the bed material. The elutriation rate is defined as follows [37]:

$$k(t) = \frac{d}{dt}W^e_{tot}(t) \tag{3}$$

The commonly used elutriation rate constant K^* is defined as follows [46]:

$$R_e(t) = 1 - e^{-\frac{K^* A}{W_0}t} \tag{4}$$

where A is the cross-sectional area of the fluidized bed (m^2).

It should be noted that, when the height above which the concentration of entrained particles remains constant or varies only slightly, this height is referred to as transport disengaging height (TDH) [47]. In

this work, the elutriation measured as a total mass loss of the bed material, thus it represents the elutriation above the TDH. The calculation of elutriation rate constant is based on results from the last 2 h of the experiment.

3.2. Agglomerate properties

In order to help improve understanding on the elutriation of nanoparticle agglomerates, the sizes of nanoparticle agglomerates at three locations are investigated, that are the bed surface, the splash zone and the bed outlet, as noted in Fig. 1.

The agglomerates at the bed surface are sampled at the top of dense bed after the bed collapse, which represent the agglomerates during fluidization. After the fluidizing gas supply is stopped and the bed collapses, then we use a slide to load samples of agglomerates on the bed surface gently, and then put the slide onto the observation platform of the microscope and measure the size of the agglomerates. During the sampling and measurement, the agglomerates are not toughed by hands. Since the main fraction of the fluidized agglomerates is in a range of tens of microns to several hundred microns and our focus here is the large agglomerates, the fine irregular agglomerates whose size less than 50 μm are not counted.

The agglomerates in the splash zone are recorded on-line by a high-speed camera with an LED-light whose one pixel is 3.9 μm in the images. As previously mentioned the accurate area referred as the "splash zone" here is actually the "top of the splash zone", where only few agglomerates that are ejected into the freeboard and the solid volume fraction is quite low, as illustrated in Fig. l.

The agglomerates at the outlet are sampled on-line using a test grid and then their size distributions are measured on the test grid without touching the agglomerates by the microscopy whose one pixel is 1.7 μm in the images.

In order to represent the bed material as much as possible, five groups are sampled at each location and analyzed. The agglomerate sizes measured for all the tests are listed in Appendix Table A1, which are represented by D50, D90, and D99. The agglomerate size is measured based on the projected area of the agglomerate. The size distributions are calculated based on the number weighted in this work.

4. Results and discussion

4.1. General fluidization behavior

In this section, the general fluidization behavior and agglomerate size are presented. Fig. 2 shows the fluidization patterns for different
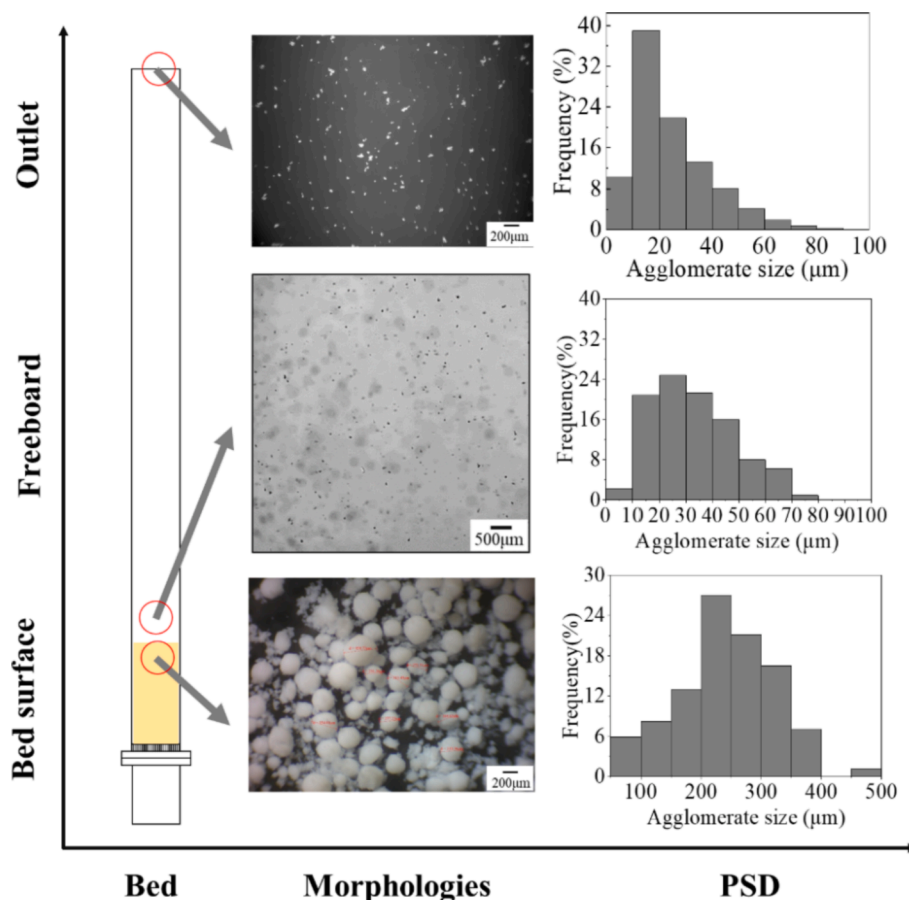
Fig. 3. Number weighted agglomerates size distributions at three positions for a typical case with $U_g = 1.0$ cm/s and $\Lambda = 23.69$ m/s^2.
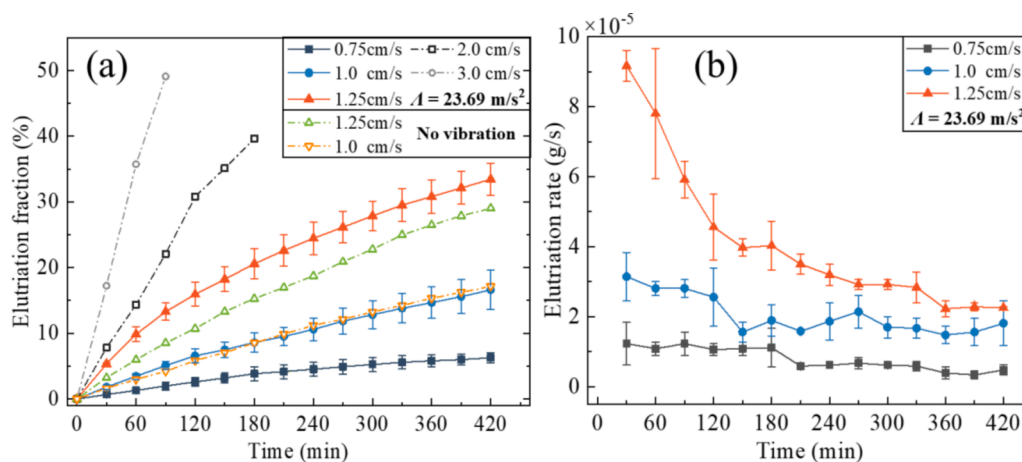

Fig. 4. (a) Cumulative elutriated fraction and (b) elutriation rate versus time for different fluidizing gas velocities at $\Lambda = 23.69$ m/s^2 and no vibration.

fluidizing gas velocities and vibration strength. For different conditions, the bed expansion ratio, H/H_0, is around 2, showing smooth fluidization. The H/H_0 increases slightly as the fluidizing gas velocity increases from 0.75 cm/s to 1.0 cm/s, while the H/H_0 no longer increases, when the fluidizing gas velocity increases to 1.25 cm/s. The H/H_0 slightly decreases as the vibration strength increases from 15.79 m/s^2 to 31.58 m/s^2. In fact, with increasing vibration strength gradually, the H/H_0 first increases, then stables and even decreases slightly, when vibration strength exceeds a critical value. In this work, the vibration strength used is larger than the critical value. The vibration can not only promote the breakage of agglomerates, but also increase the collision velocity

and contact area between agglomerates which could make the agglomerates larger and denser [19]. Moreover, the increased vibration strength results in more intense fluctuation of the bed surface, which could increase the entrainment of the agglomerates from the bed.

Fig. 3 shows the size distribution of the agglomerates at three locations, for a typical case ($U_g = 1.0$ cm/s, $\Lambda = 23.69$ m/s^2). The size distributions at the bed surface, in the splash zone, and at the bed outlet are mainly around $50 - 400$ μm, $10 - 70$ μm, $10 - 60$ μm, respectively. The agglomerates in dense bed, from several tens to a few hundreds of microns, are during continuously colliding, breaking, and recombining. The agglomerates on the bed surface are ejected from the dense bed into
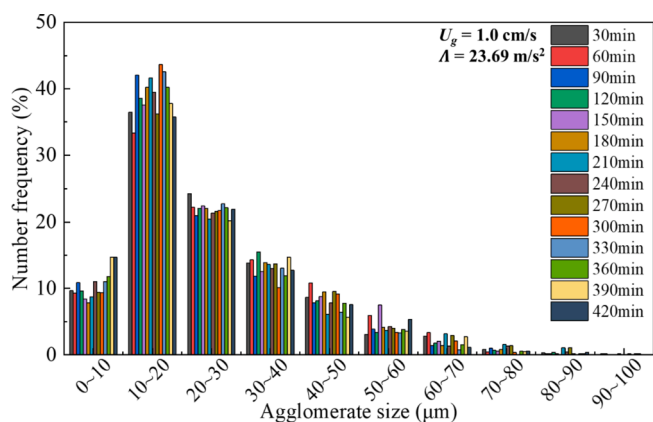
Fig. 5. Number weighted size distributions of elutriation agglomerates at different times for the case with $U_g = 1.0$ cm/s and $\Lambda = 23.69$ m/s².

the splash zone. Then, the small agglomerates in the splash zone could be entrained onto freeboard and then elutriated out of the bed or fall back into the dense bed, depending on their sizes. The quantitative results will be discussed in detail in the following sections.

4.2. Effect of fluidizing gas velocity on elutriation

Fig. 4 (a) shows the cumulative fraction of the elutriated agglomerates over time for different fluidizing gas velocities at $\Lambda = 23.69$ m/s². The elutriated fraction increases with increase of fluidizing gas velocity. The mass loss is about 5% at $U_g = 0.75$ cm/s after fluidization of 7 h, while it reaches more than 33% at $U_g = 1.25$ cm/s. Note that the two dotted lines in Fig. 4 (a) are the elutriated fraction at even higher fluidizing gas velocities. The mass loss of the bed material has even reached 50% after 90 min at $U_g = 3$ cm/s. This suggests that fluidization with high fluidizing gas velocity is not favorable. The elutriation under conditions without vibration assistance is also measured. Results show that the elutriation fraction under $U_g = 1.25$ cm/s without vibration after 7 h is around 30%, slightly smaller the condition with vibration. The bed expansion ratio is also smaller, around 1.3. Because under conditions without vibration, the bed fluctuation is lighter and fewer agglomerates are ejected into the freeboard. At $U_g = 1.0$ cm/s, the elutriation without vibration is almost identical to that with vibration, around 17%. The fluidization state without vibration is not stable at $U_g = 1.0$ cm/s, and the bed surface is occasionally unstable. If U_g is further decreased to 0.75 m/s, the fluidization is not very smooth without the assistance of vibration, but the fluidization is improved significantly

under the vibration. Therefore, the elutriation at $U_g = 0.75$ cm/s with aeration alone is not measured.

It can be seen in Fig. 4 (b) that, the elutriation rate first decreases with time and then gradually stabilizes after about 3 h. The initial elutriation rate is influenced by the initial agglomerates presented in the fluidized bed. After a period of fluidization, the agglomerates are under continuously breaking and recombining, which leads to more stable units of agglomerates, thus the elutriation rate is decreased first and then stable. This is similar to the ordinary particles where the abrasion of particles is not neglected [41,42,45,48,49].

Fig. 5 shows the size distribution of the elutriated agglomerates at different times for a typical case with $U_g = 1.0$ cm/s and $\Lambda = 23.69$ m/s². The results show that the size distribution of the agglomerates does not change significantly with time, with the main fraction of agglomerates being approximately 20 μm, which indicates that the size distribution of the elutriated agglomerates is nearly steady with time.

Fig. 6 (a) shows the number weighted size distributions averaged over time of the elutriated agglomerates under different fluidizing gas velocities. The size of the elutriated agglomerates is mainly in the range of $10 - 30$ μm. The proportion of small agglomerates is higher at the low fluidizing gas velocity, while the proportion of large agglomerates is higher with increase of fluidizing gas velocity. The D99 of the agglomerates size is 47 μm, 67 μm, 69 μm for fluidizing gas velocity of 0.75 cm/s, 1.0 cm/s, 1.25 cm/s, respectively (Table A1). This coincides with the freefall tests of agglomerates, which shows that the terminal velocity of the agglomerates of 60 μm and 80 μm is around 0.75 cm/s and 1.25 cm/s, respectively.

Fig. 6 (b) shows the number average size of the elutriated agglomerates with time. The results show the average size of elutriated agglomerates is in the range of $10 - 30$ μm, and fluctuates around a steady value. The average agglomerate size at $U_g = 0.75$ cm/s is lower than that for the higher gas velocities, which is as expected. The difference of agglomerates size between the conditions at $U_g = 1.0$ cm/s and $U_g = 1.25$ cm/s is neglected except for the latter 1.5 h of the test. A possible reason is speculated in the following. For $U_g = 1.25$ cm/s, the loss of bed material reaches 30% for the latter 1.5 h. After long-time fluidization, the number of small agglomerates decreases, which results in the increase of the average size.

4.3. Effect of vibration on elutriation

Vibration can improve fluidization of nanoparticle agglomerates. It can also affect the size distribution of the agglomerates in the bed and the fluctuation of the bed surface, which could cause more fines to be ejected above the bed surface and promotes the elutriation. Fig. 7 shows that the effect of changing the vibration strength on the elutriation
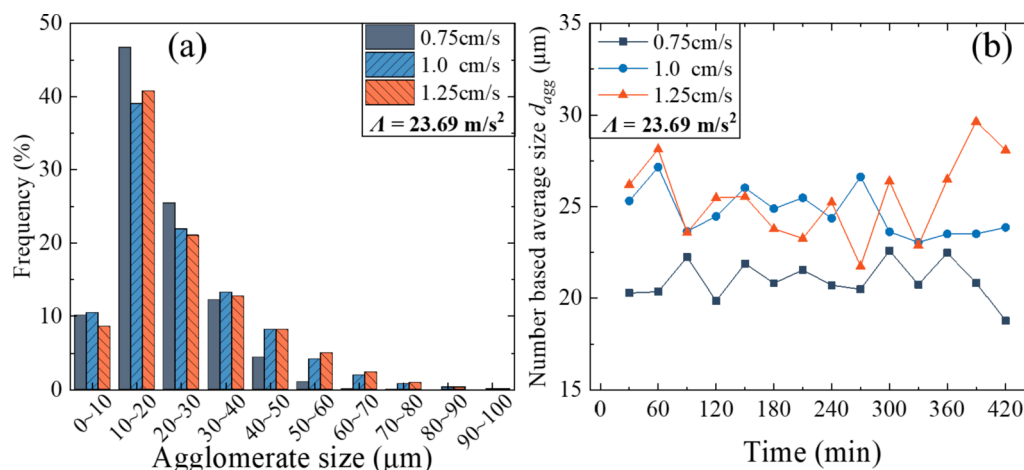

Fig. 6. (a) Size distributions and (b) number average sizes of agglomerates for different fluidizing gas velocities at $\Lambda = 23.69$ m/s².
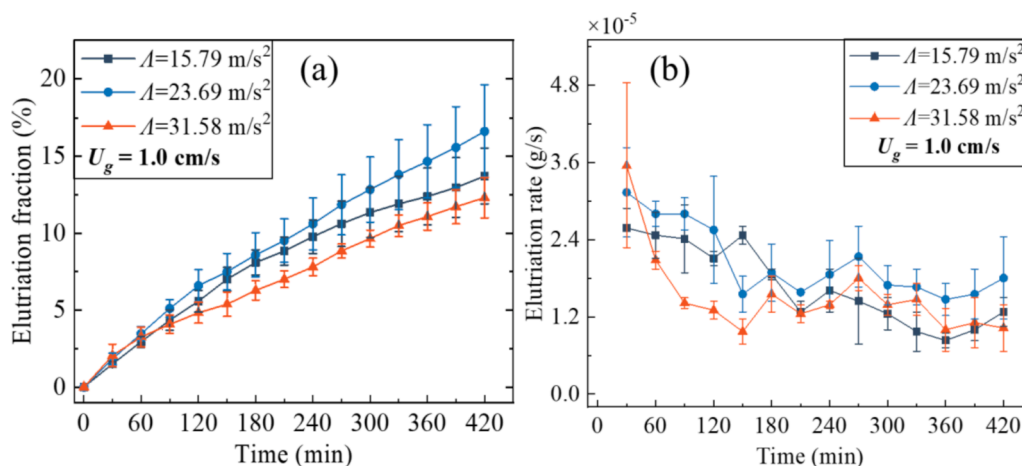
Fig. 7. (a) Cumulative entrainment fraction and (b) entrainment rate for different vibration strength at $U_g = 1.0$ cm/s.
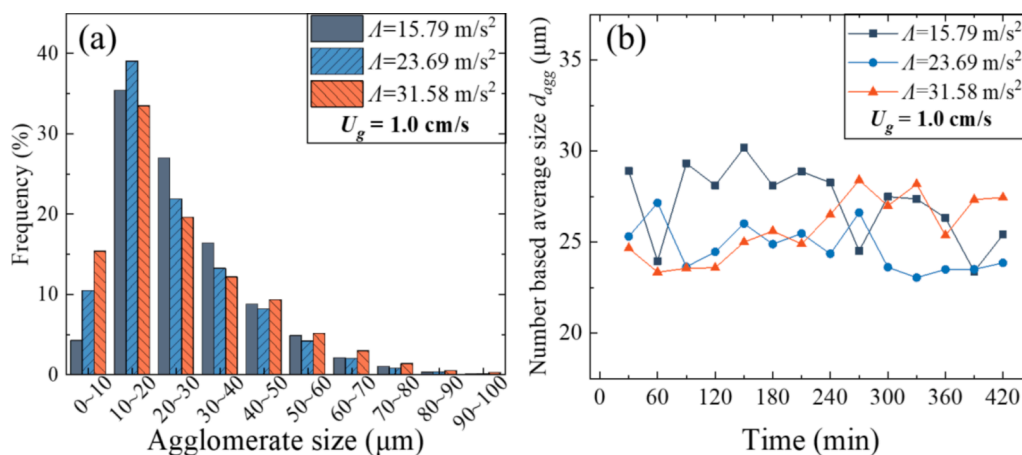

Fig. 8. (a) Size distributions and (b) number average sizes of agglomerates for different vibration strength at $U_g = 1.0$ cm/s.

fraction and elutriation rate. The results show that the increase or decrease of the vibration strength slightly reduces the total elutriated agglomerates. The total mass loss is in a range of 10%− 17% after 7 h of fluidization. As the vibration strength decreases, the fluctuation of the bed is reduced, which results in fewer agglomerates being ejected into the freeboard. At stronger vibration strength, although the large agglomerates are ejected into the freeboard, they fall in the freeboard and probably adhere to smaller agglomerates and fall back into the bed again. This can explain that the elutriation decreases when the vibration strength increases.

Fig. 8 shows the number weighted size distributions and average sizes of the elutriation agglomerates for different vibration strength at $U_g = 1.0$ cm/s. The main fraction is in the range of $10 − 30$ μm, with the D99 of 70 μm approximately. For $\Lambda = 31.58$ m/s^2, there are more large agglomerates than for the weaker vibration strength. This is probably because the stronger vibration causes more agglomerates being ejected into the freeboard. It can also be observed that the average size of the elutriated agglomerates becomes larger with time at the vibration strength of $\Lambda = 31.58$ m/s^2, which indicates that the agglomeration is promoted under the stronger vibration.

4.4. Agglomerate behavior

The significant difference between fluidization of nanoparticles and "ordinary" particles of tens of microns is that nanoparticles are present in the form of agglomerates. The properties of the agglomerates are extremely different from those of the primary particles. Therefore, the

morphology of agglomerates needs to be studied for interpreting the elutriation behavior.

Fig. 9 shows that most of the agglomerates ejected into the splash zone are in the range of $10 − 50$ μm for different fluidizing gas velocities at $\Lambda = 23.69$ m/s^2. During the experiment, it can be observed that some large agglomerates are moving upward and downward continuously in the splash zone. As expected, more and larger agglomerates are ejected as the fluidizing gas velocity increasing. When the fluidizing gas velocity is 0.75 cm/s, 1.0 cm/s, and 1.25 cm/s, the D99 of the agglomerates size is 54 μm, 65 μm, and 75 μm, respectively.

The agglomerates are ejected into the splash zone due to drag by the gas and the vibration of bed. Since the local gas velocity could be larger than the fluidizing gas velocity, the agglomerates whose terminal velocity larger than the fluidizing gas velocity could also be entrained. Nevertheless, the entrained large agglomerates will fall back into the bed again as the local gas velocity drops in the freeboard. Moreover, the elutriated agglomerates still could collide and agglomerate to form larger agglomerates during the upward movement in the freeboard. These agglomerates could be elutriated or fall back into the dense bed depending on their sizes.

Fig. 10 shows that the number and size of agglomerates ejected into the splash zone increases as the vibration strength at $U_g = 1.0$ cm/s, and the largest proportion of agglomerates is still in the range of $10 − 50$ μm. Based on the images shown in Fig. 10, some agglomerates are moving upward and downward continuously in the splash zone. As the vibration strength increases, the chance of agglomerate collision and adhesion increases. This promotes the result shown in Fig. 7(b) that the elutriation
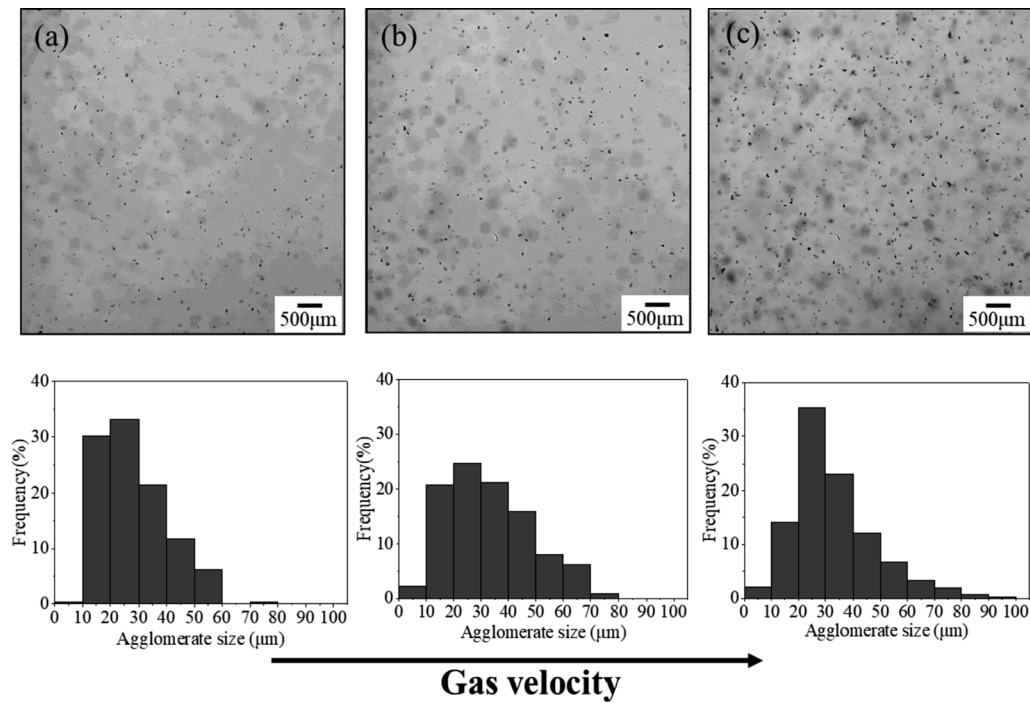
Fig. 9. Agglomerate images and size distributions in the splash zone for different fluidizing gas velocities at $\Lambda = 23.69$ m/s^2, (a) $U_g = 0.75$ cm/s, (b) $U_g = 1.0$ cm/s, (c) $U_g = 1.25$ cm/s.
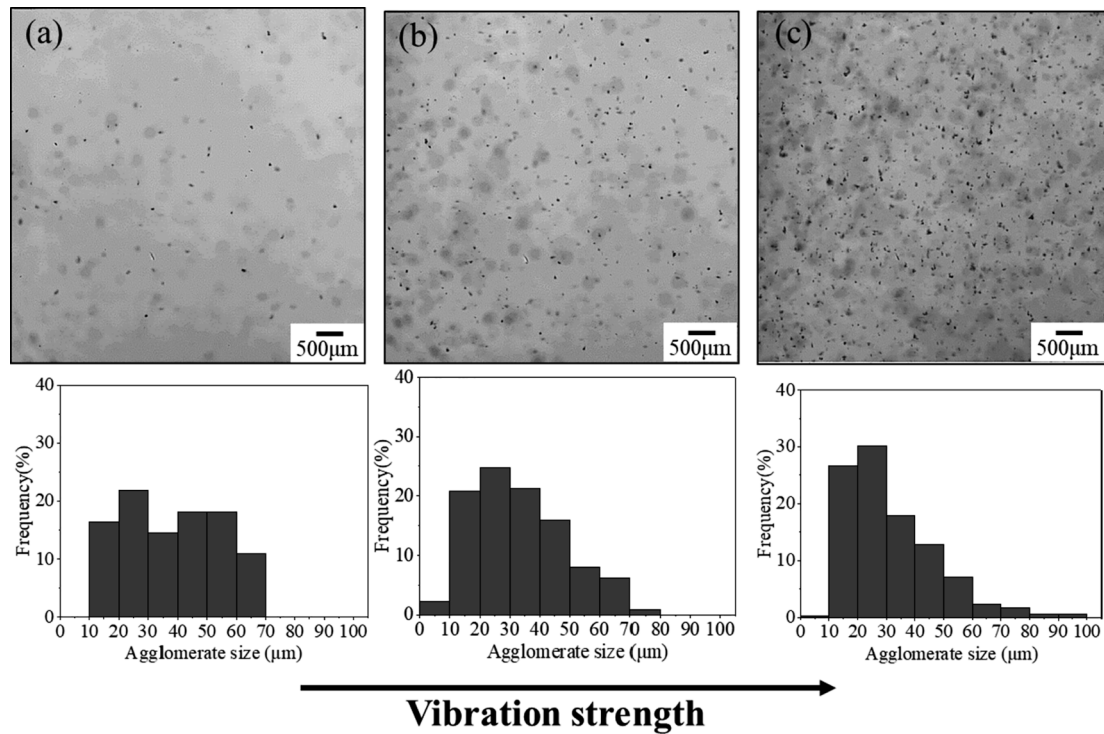

Fig. 10. Agglomerate images and size distributions in the splash zone for different vibration strength at $U_g = 1.0$ cm/s, (a) $\Lambda = 15.79$ m/s^2, (b) $\Lambda = 23.69$ m/s^2, (c) $\Lambda = 31.58$ m/s^2.

rate decreases slightly with increase of vibration strength.

Fig. 11 and Fig. 12 show the sizes of the agglomerates sampled at the bed surface, after the bed collapse. These agglomerates are in the range from tens of microns to several hundred microns, called complex agglomerates in the literature [5]. When the complex agglomerates break and recombine in the fluidized bed, small agglomerates created during

this process may be ejected into zone above the bed surface and are then elutriated by the fluidizing gas.

The agglomerates at the bed surface are larger at higher fluidizing gas velocity, while the number of small agglomerates that can be elutriated does not differ significantly for different fluidizing gas velocities (Fig. 11). The number of small agglomerates increases with the
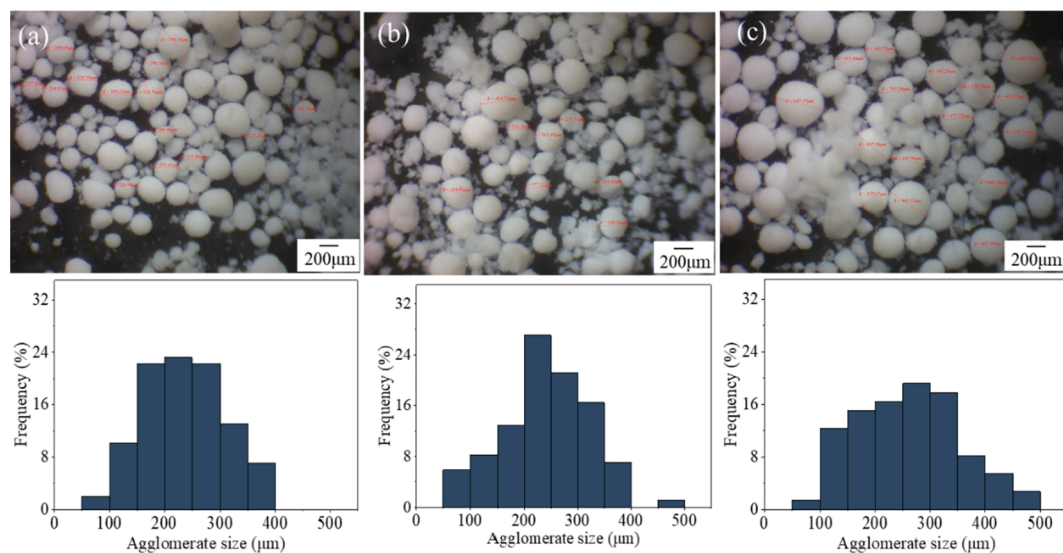
Fig. 11. Agglomerate images and size distributions at bed surface for different fluidizing gas velocities at $\Lambda = 23.69$ m/s^2, (a) $U_g = 0.75$ cm/s, (b) $U_g = 1.0$ cm/s, (c) $U_g = 1.25$ cm/s.
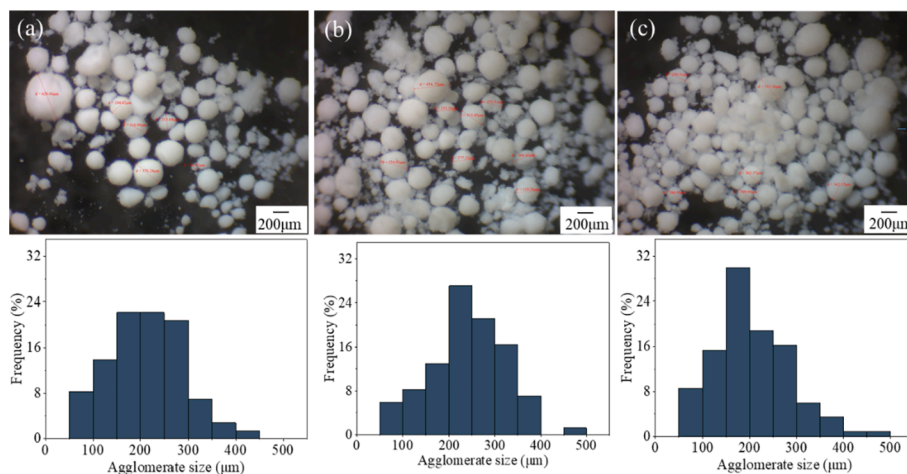

Fig. 12. Agglomerate images and size distributions at the bed surface for different vibration strength at $U_g = 1.0$ cm/s, (a) $\Lambda = 15.79$ m/s^2, (b) $\Lambda = 23.69$ m/s^2, (c) $\Lambda = 31.58$ m/s^2.
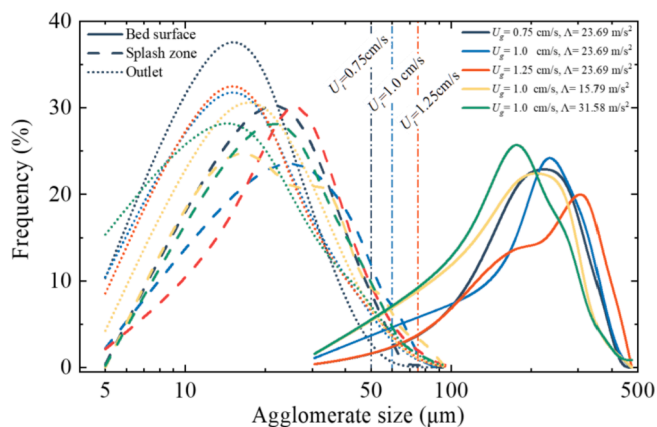

Fig. 13. Agglomerate size distributions at the bed surface, splash zone and outlet.

vibration strength (Fig. 12), since the strong vibration enhances fluctuation of the bed which causes the large complex agglomerates to break up to produce more small agglomerates. These results show that the effect of changing vibration is more obvious for the agglomerates within the dense bed.

Although the off-line is employed in this work, the agglomerate size at the bed surface is generally in line with the results other studies. In the literature, the agglomerate size is measured extensively using different methods, including both on-line and off-line methods. Valverde et al. [16]. summarizes the studies on agglomerate size in nanofluidized beds and showed that the size of SiO$_2$ agglomerates is around 200 μm to 300 μm. In particular, Quevedo et al. [50] measured the agglomerate size in situ by using modified particle vision probes, and reported that the mean sizes for hydrophobic silica R974 nanoparticles under conventional fluidized bed are around 100–250 μm, respectively. Zhu et al. [13]. measured the size of agglomerates within the nanofluidized bed (Degussa AerosilR R974) in the range of 200–600 μm using an in-line camera method.
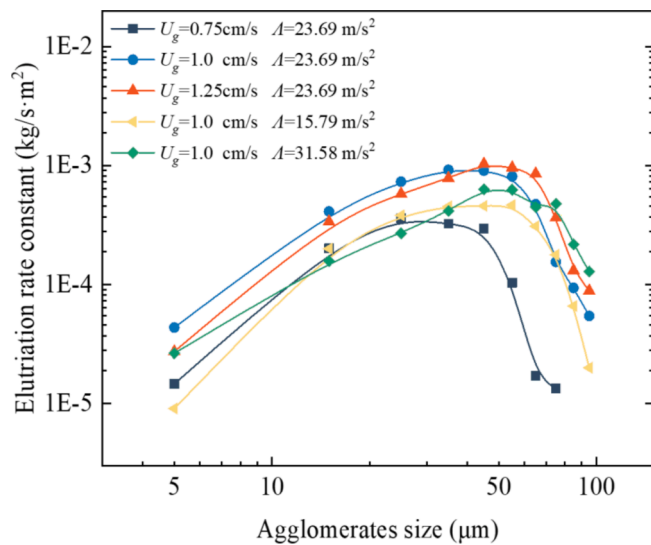
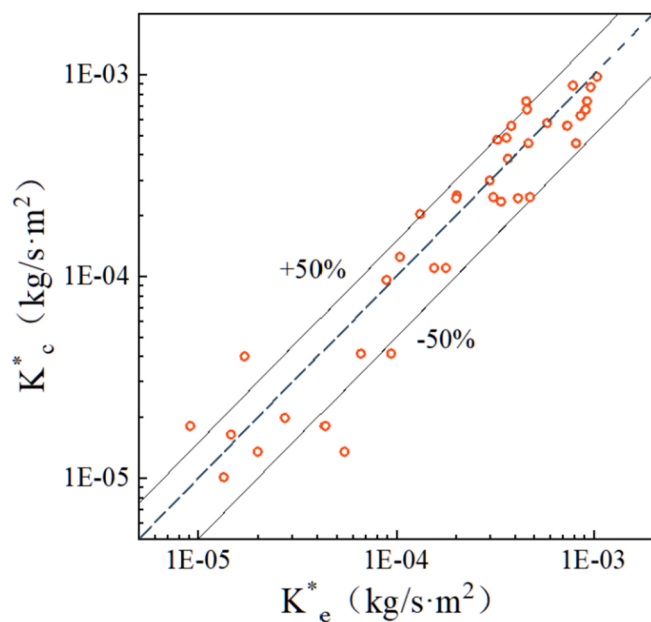**Fig. 14.** Elutriation rate constant versus agglomerates size.

Fig. 15. Comparison of experimental elutriation rate constant with those calculated from the empirical correlation of Eq. (7).

4.5. Elutriation mechanism with agglomerates

Fig. 13 summarizes the agglomerate size distributions at different locations for different conditions. The solid lines, dash lines and dotted lines are the agglomerate size distributions at the bed surface, splash zone, and outlet, respectively. Evolution of agglomerate size at the three locations helps us to understand the elutriation of the nanoparticle agglomerates. During fluidization, nanoparticles form the complex agglomerates in the range of tens of microns to several hundreds of microns. Some small agglomerates are formed due to breakup and recombination of the complex agglomerates. When the bed surface fluctuates, some small agglomerates are ejected above the bed surface. The size distribution of the agglomerates during the entrainment process in the splash zone is in the range of $5-100\ \mu m$. When the gas velocity is larger than the terminal velocity of the agglomerates, the agglomerates are elutriated and move upwards. Meanwhile, the agglomerates may adhere to form new larger agglomerates during their movement in the

freeboard, which can fall back into the dense bed again. Some upward flowing agglomerates could adhere to the bed wall, which would fall off due to vibration. Then, the remaining agglomerates are elutriated through the outlet, whose size distribution is in the range of about $5-80\ \mu m$.

Fig. 14 shows the relationship between elutriation rate constant and agglomerates size, d_{agg}, under different conditions. The result shows that as the size of the elutriated agglomerates increases from $5\ \mu m$ to $100\ \mu m$, the elutriation rate constant increases first and then decreases. The turning point corresponds to the size around $45\ \mu m$. The decrease of elutriation rate constant for fine agglomerate is also reported in the elutriation process of the group C particles, where the elutriation constant gradually plateaus or even decreases as the particle size decreases to a critical size [37–39,42,44]. Eqs. (5) and (6) for determining the critical size were proposed by Ma [39] and Li [37], respectively.

$$d_p^* = \frac{91}{900\rho_p^{0.731}g} \tag{5}$$

$$d_p^* = \frac{101}{100\rho_p g^{0.731}} \tag{6}$$

where d_p^* is the critical particle diameter, and ρ_p is the particle density.

In this work, the particle properties in Eqs. (5) and (6) should be replaced by the agglomerate properties. The critical sizes calculated from Eqs. (5) and (6) are $37\ \mu m$ and $9\ \mu m$, respectively. The result of $37\ \mu m$ calculated by Eq. (5) agrees well with the phenomena in this work. The common explanation is that the strong adhesion causes the small agglomerates to adhere into the larger agglomerates which inhibits the elutriation of the small agglomerates [37,39,44]. Nanoparticle agglomerates consist of very adhesive primary particles and therefore the small elutriation rate constant for the small agglomerates is more pronounced compared to the ordinary particles. Moreover, for nanoparticle fluidized beds, another reason causes this result. As can be seen from Figs. 9 and 10, the small agglomerates which are smaller than $25\ \mu m$ in the splash zone are few. Therefore, because the number of small agglomerates produced is relatively low, the elutriation rate constant of the small agglomerates is low.

It should be noted that the elutriation rate constant in this work is approximately two orders of magnitude smaller than the previously reported results. The two main reasons are follows. First, the fluidizing gas velocity in this study is around $0.01\ m/s$, which is much smaller than that of the ordinary particles under fluidizing gas velocity with approximately $0.1\ m/s - 1.5\ m/s$ [39,42,43,51,52]. The fluidizing gas velocity is the most significant factor affecting the elutriation rate constant. Second, the elutriable agglomerates that produced by breaking up of complex aggregates are not significant. In addition, for the same size agglomerates with the ordinary particles, the density of the agglomerates is much smaller than that of the ordinary particles, which causes the mass of the agglomerates is small.

4.6. Correlation of elutriation rate constant

In previous studies, some empirical correlations for the elutriation rate constant applicable to the group C particles have been proposed, as listed in Table A2 [37,39,42,43,51,52]. However, these correlations do not give a good fit for nanoparticle agglomerates. Based on these correlations, the fluidizing gas velocity, agglomerate density and size are used as input parameters. Moreover, the elutriation rate constant for different sizes of agglomerates is different, which depends on the critical size. In this work, a Gaussian distribution is used to fit distribution of elutriation rate constant. The critical size is chosen based on the size of agglomerates whose terminal velocity is equal to the fluidizing gas velocity. By using regression analysis, a correlation is proposed as Eq. (7). The agglomerate density, ρ_{agg}, is also used as input parameters because the agglomerate density varies with their sizes.

$$K^* = 4.62 \times 10^{-4} U_g^{1.572} \left[\frac{(\rho_{agg} - \rho_g)g}{18\mu} \right]^{\frac{1}{2}} \times$$

$$\exp\left\langle -2.77 \left\{ 1.584 - 1.8 \times 10^{-6} \left[\frac{d_{agg}^2 (\rho_{agg} - \rho_g)g}{18\mu U_g} \right]^{\frac{1}{2}} \right\}^2 \right\rangle \tag{7}$$

The correlation is valid in range of $U_g = 0.65 - 1.3$ cm/s, $d_{agg} = 5 - 100$ μm, which are the experimental conditions in this work. A comparison of the experimental results with the calculated values by Eq. (7) is shown in Fig. 15, showing good agreement. The significance of the current correlation lies in that it indicates the elutriation rate constant for nanoparticle agglomerates is related to the parameters in Eq. (7), but the validation of the quantitative relationship in other situations requires further investigation. In particular, the elutriation rates in fluidized beds with different diameters still need more investigation. In this work, the influence of the bed wall is minimized as much as possible. We have coated both the inner and outer walls of the fluidized bed with an electrostatic eliminator to minimize the effect of the electric adhesion. The fluidization is almost homogeneous (Fig. 2), no significant large bubbles are observed and therefore the bubble motion is not significantly restricted. Therefore, the elutriation rate constant obtained in this paper are, to a certain extent, applicable to fluidized beds with larger diameters. It is meaningful to test the applicability of the elutriation rate constant obtained in the small fluidized bed to the larger fluidized beds in future study.

5. Conclusions

In this work, we carried out elutriation experiments on silica nanoparticle agglomerates in a vibro-fluidized bed. The agglomerates morphology and size distributions at the bed surface, splash zone, and bed outlet are studied. The main conclusions are listed as following:

1. Among conditions with different fluidizing gas velocities and vibration strength, the lowest elutriation fraction is measured around 5% after 7-hour fluidization.

2. Fluidizing gas velocity has a great influence on the elutriation of the nanoparticle agglomerates. The elutriation rate constant and the elutriated agglomerates size increase with fluidizing gas velocity.

3. The effect of varying the vibration strength on elutriation rate is not significant compared to varying the fluidizing gas velocity. However, the increase of vibration strength enhances the bed fluctuation, which causes more agglomerates being ejected into the splash zone. The increased vibration strength also increases the number of agglomerates that can be elutriated in the bed.

4. As the agglomerate size decreases, the elutriation rate constant first increases and then decreases. The decrease of elutriation rate constant is due to the strong adhesion, which leads fine agglomerates adhered into larger agglomerates.

5. The elutriation rate constant of the nanoparticle agglomerates is much smaller than the ordinary particles due to the low fluidizing gas velocity and agglomerate density. An empirical correlation considering agglomerate size distribution is proposed and fitted well with the elutriation rate constant of the current experimental conditions.

Finally, we remark that it is more challenging to develop a general physical model of the elutriation rate constant for nanoparticle agglomerates, but it should be the pursuit in future study.

Declaration of Competing Interest

The authors declare that they have no known competing financial interests or personal relationships that could have appeared to influence the work reported in this paper.

Appendix A. Test of agglomerate density

The agglomerate density is determined by measuring the terminal velocity of agglomerates [53] in a freefall test. When the agglomerate reaches the terminal velocity after released at a certain height, the drag force on the agglomerate and the gravity force are balanced. Based on the Stokes Law the terminal velocity is as follows:

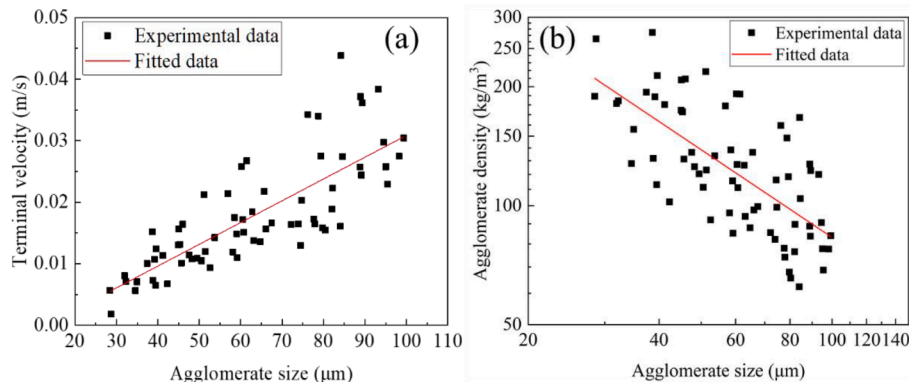$$U_t = \left[\frac{4}{3} \frac{d_{agg}(\rho_{agg} - \rho_g)g}{\rho_g C_D} \right]^{\frac{1}{2}} \tag{8}$$

Fig. A1. Experimental and fitted values of agglomerate terminal velocity and density as a function of agglomerate size.

where U_t is the terminal velocity, d_{agg} the agglomerate diameter, ρ_{agg} the agglomerate density, ρ_g the fluid density, g the gravity, and C_D the drag coefficient. When the Reynolds number of the particles satisfies Re less than 1, then $C_D = 24/Re$. Thus, Eq. (8) is simplified to the following:

$$U_t = \frac{d_{agg}^2(\rho_{agg} - \rho_g)g}{18\mu} \tag{9}$$

where μ is the fluid viscosity.

Fig. A1 (a) and Fig. A1 (b) show the terminal velocity and density of the agglomerates as a function of agglomerate size, respectively. The linear fit in a logarithmic coordinate system gives a fitted curve with a slope of -0.7, thus the fractal dimension of the agglomerates is around 2.3, which is similar to the results reported by de Martín [18]. The agglomerate density is in a range of around $250 - 60 \text{ kg/m}^3$ for the size of $30 - 100 \text{ μm}$.

Appendix B. Summary of agglomerate size under different conditions

Table A1
Agglomerates size of D50, D90, D99 under different conditions.

Condition	Location	D50 (μm)	D90 (μm)	D99 (μm)
$U_g = 0.75$ cm/s, $\Lambda = 23.69$ m/s^2	bed surface	209	314	368
	splash zone	21	42	54
	outlet	21	31	47
$U_g = 1.0$ cm/s, $\Lambda = 23.69$ m/s^2	bed surface	217	320	433
	splash zone	26	51	65
	outlet	24	42	67
$U_g = 1.25$ cm/s, $\Lambda = 23.69$ m/s^2	bed surface	250	362	412
	splash zone	25	50	75
	outlet	27	44	69
$U_g = 1.0$ cm/s, $\Lambda = 15.79$ m/s^2	bed surface	186	284	390
	splash zone	25	54	80
	outlet	26	43	69
$U_g = 1.0$ cm/s, $\Lambda = 31.58$ m/s^2	bed surface	169	284	417
	splash zone	23	58	76
	outlet	27	35	73

Note: the D50, D90, D99 are number based.

Appendix C. Summary of agglomerate size under different conditions

Table A2
Typical published correlations for elutriation rate constant of group C.

Year	Authors	Correlations
1980	Lin et al., [52]	$K_{i\infty} = 9.43 \times 10^{-4}\rho_g U_g \left(\dfrac{U_g^2}{gd_{pi}}\right)^{1.65}$
1987	Geldart and Wong [51]	$K_{i\infty} = 13.52\rho_g U_g \exp\left(-30.3\dfrac{U_{ti}}{U_g}\right)$
1998	Ma and Kato [39]	$K_{i\infty} = 5.38\rho_g(U_g - U_{ti})\left(\dfrac{d_{pi}(U_g - U_{ti})\rho_g}{\mu_g}\right)^{2.22}\left(\dfrac{0.455\rho_g^{0.269}}{\rho_g g d_{pi}}\right)^{-0.15}$ for $d_{pi} < \dfrac{0.455\rho_g^{0.269}}{4.5g\rho_p}$
2000	Rodriguez et al., [42]	$K_{i\infty} = \dfrac{\mu_g(U_g - U_{ti})^2(1.5 \times 10^{-9}Re_{ti}^{0.6} + 2.5 \times 10^{-5}Re_{ti}^{1.2})}{gd_{pi}^2}$
2001	Li and Kato [37]	$K_{i\infty} = 6.64 \times 10^6 C_{ps}\left(\dfrac{\rho_g U_g g}{\rho_p}\right)^{2.64}$ for $d_{pi} \leq d_{crit}$, $C_{ps} = \begin{cases} 1 \text{ for } d_{pi} < 60\mu m \\ \left(\dfrac{200 - d_{pi}}{150}\right)^\alpha + \left(\dfrac{d_{pi} - 60}{150}\right)^\alpha \\ \left(\dfrac{d_{pi}}{d_{crit}}\right)^{1.4} \text{ for } 60\mu m \leq d_{pi} \leq 200\mu m \\ \left(\dfrac{d_{pi}}{d_{crit}}\right)^{1.4} \text{ for } d_{pi} \geq 200\mu m \end{cases}$ $\alpha = \left(\dfrac{d_{crit}}{d_{pi}}\right)^{0.3}, d_{crit} = \dfrac{1.01 \times 10^5}{\rho_p g^{0.731}}$
2005	Chang et al., [43]	$K_{i\infty} = 0.0136\rho_g U_{ti}\dfrac{Fr^{1.25}}{\left(\dfrac{T_{bed}}{T_{ambient}}\right)^{0.31}}$

References:

[1] A.T. Bell, The impact of nanoscience on heterogeneous catalysis, Science 299 (5613) (2003) 1688–1691.

[2] T.-T. Hu, J.-X. Wang, Z.-G. Shen, J.-F. Chen, Engineering of drug nanoparticles by HGCP for pharmaceutical applications, Particuology 6 (4) (2008) 239–251.

[3] P.S. Nayak, S.M. Borah, H. Gogoi, S. Asthana, R. Bhatnagar, A.N. Jha, S. Jha, Lactoferrin adsorption onto silver nanoparticle interface: Implications of corona on protein conformation, nanoparticle cytotoxicity and the formulation adjuvanticity, Chem. Eng. J. 361 (2019) 470–484.

[4] B.D. Martin, L. De Kock, T. Stephenson, S.A. Parsons, B. Jefferson, The impact of contactor scale on a ferric nanoparticle adsorbent process for the removal of phosphorus from municipal wastewater, Chem. Eng. J. 215-216 (2013) 209–215.

[5] Y. Wang, G. Gu, F. Wei, J. Wu, Fluidization and agglomerate structure of SiO_2 nanoparticles, Powder Technol. 124 (2002) 152–159.

[6] H. Liu, S. Wang, Fluidization behaviors of nanoparticle agglomerates with high initial bed heights, Powder Technol. 388 (2021) 122–128.

[7] X. Zhu, Q. Zhang, Y. Wang, F. Wei, Review on the nanoparticle fluidization science and technology, Chinese, J Chem. Eng. 24 (1) (2016) 9–22.

[8] M.R. Tamadondar, R. Zarghami, M. Tahmasebpoor, N. Mostoufi, Characterization of the bubbling fluidization of nanoparticles, Particuology 16 (2014) 75–83.

[9] S. Salameh, J. Schneider, J. Laube, A. Alessandrini, P. Facci, J.W. Seo, L.C. Ciacchi, L. Mädler, Adhesion Mechanisms of the Contact Interface of TiO_2 Nanoparticles in Films and Aggregates, Langmuir 28 (31) (2012) 11457–11464.

[10] J.R. van Ommen, J.M. Valverde, R. Pfeffer, Fluidization of nanopowders: a review, J. Nanopart. Res. 14 (3) (2012), https://doi.org/10.1007/s11051-012-0737-4.

[11] S. Kaliyaperumal, S. Barghi, J. Zhu, L. Briens, S. Rohani, Effects of acoustic vibration on nano and sub-micron powders fluidization, Powder Technol. 210 (2) (2011) 143–149.

[12] J. Quevedo, R. Pfeffer, Y. Shen, R. Dave, H. Nakamura, S. Watano, Fluidization of nanoagglomerates in a rotating fluidized bed, AIChE J. 52 (7) (2006) 2401–2412.

[13] C. Zhu, Q. Yu, R.N. Dave, R. Pfeffer, Gas fluidization characteristics of nanoparticle agglomerates, AIChE J. 51 (2) (2005) 426–439.

[14] J. Jung, D. Gidaspow, Fluidization of nano-size particles, J. Nanopart. Res. 4 (2002) 483–497.

[15] A. Fabre, S. Salameh, M.T. Kreutzer, J.R. van Ommen, Modeling the size distribution in a fluidized bed of nanopowder, Powder Technol. 312 (2017) 347–353.

[16] J.M. Valverde, A. Castellanos, Fluidization, bubbling and jamming of nanoparticle agglomerates, Chem. Eng. Sci. 62 (23) (2007) 6947–6956.

[17] Q. Yu, R.N. Dave, C. Zhu, J.A. Quevedo, R. Pfeffer, Enhanced fluidization of nanoparticles in an oscillating magnetic field, AIChE J. 51 (7) (2005) 1971–1979.

[18] L. de Martín, A. Fabre, J. Ruud van Ommen, The fractal scaling of fluidized nanoparticle agglomerates, Chem. Eng. Sci. 112 (2014) 79–86.

[19] Z. Zhao, D. Liu, J. Ma, X. Chen, Fluidization of nanoparticle agglomerates assisted by combining vibration and stirring methods, Chem. Eng. J. 388 (2020), 124213.

[20] J.-R. Lee, N. Hasolli, K.-S. Lee, K.-Y. Lee, Y.-O. Park, Fluidization of fine powder assisted by vertical vibration in fluidized bed reactor, Korean J. Chem. Eng. 36 (9) (2019) 1548–1556.

[21] A.A. Esmailpour, N. Mostoufi, R. Zarghami, An improved model for estimating fractal structure of silica nano-agglomerates in a vibro-fluidized bed, Int. J. Multiphys. 9 (4) (2015) 325–340.

[22] X. Liang, H. Duan, T. Zhou, J. Kong, Fluidization behavior of binary mixtures of nanoparticles in vibro-fluidized bed, Adv. Powder Technol. 25 (1) (2014) 236–243.

[23] S. Kaliyaperumal, S. Barghi, L. Briens, S. Rohani, J. Zhu, Fluidization of nano and sub-micron powders using mechanical vibration, Particuology 9 (3) (2011) 279–287.

[24] H. Wang, T. Zhou, J.-S. Yang, J.-J. Wang, H. Kage, Y. Mawatari, Model for Calculation of Agglomerate Sizes of Nanoparticles in a Vibro-fluidized Bed, Chem. Eng. Technol. 33 (3) (2010) 388–394.

[25] J. Yang, T. Zhou, L. Song, Agglomerating vibro-fluidization behavior of nano-particles, Adv. Powder Technol. 20 (2) (2009) 158–163.

[26] D. Barletta, G. Donsì, G. Ferrari, M. Poletto, P. Russo, The effect of mechanical vibration on gas fluidization of a fine aeratable powder, Chem. Eng. Res. Des. 86 (4) (2008) 359–369.

[27] E.K. Levy, B. Celeste, Combined effects of mechanical and acoustic vibrations on fluidization of cohesive powders, Powder Technol. 163 (1-2) (2006) 41–50.

[28] C.H. Nam, R. Pfeffer, R.N. Dave, S. Sundaresan, Aerated vibrofluidization of silica nanoparticles, AIChE J. 50 (8) (2004) 1776–1785.

[29] C.Y. Wen, L.H. Chen, Fluidized bed freeboard phenomena: Entrainment and elutriation, AIChE J. 28 (1) (1982) 117–128.

[30] J.W. Chew, A. Cahyadi, C.M. Hrenya, R. Karri, R.A. Cocco, Review of entrainment correlations in gas–solid fluidization, Chem. Eng. J. 260 (2015) 152–171.

[31] A. Dutta, L.V. Dullea, Effects of external vibration and the addition of fibers on the fluidization of a fine powder, AIChE Symp. Ser. 281 (1991) 38–46.

[32] C. Zhu, G. Liu, Q. Yu, R. Pfeffer, R.N. Dave, C.H. Nam, Sound assisted fluidization of nanoparticle agglomerates, Powder Technol. 141 (1-2) (2004) 119–123.

[33] A. Fabre, A. Clemente, F. Balas, M.P. Lobera, J. Santamaría, M.T. Kreutzer, J.R. van Ommen, Entrainment of nanosized clusters from a nanopowder fluidized bed, Environmental Science, NANO 4 (2017) 670–678.

[34] D. Kunii, O. Levenspiel, Entrainment of Solids from Fluidized Beds I. Hold-Up of Solids in the Freeboard II. Operation of Fast Fluidized Beds, Powder Technol. 61 (2) (1990) 193–206.

[35] T. Baron, J.D. Hazlett, M.A. Bergougnou, C.L. Briens, P. Galtier, Size distribution of the particles entrained from fluidized beds: Gas humidity effects, Can. J. Chem. Eng. 70 (4) (1992) 631–635.

[36] J. Baeyens, D. Geldart, S.Y. Wu, Elutriation of fines from gas fluidized beds of Geldart A-type powders - effect of adding superfines, Powder Technol. 71 (1) (1992) 71–80.

[37] J. Li, K. Kato, A correlation of the elutriation rate constant for adhesion particles (group C particles), Powder Technol. 118 (3) (2001) 209–218.

[38] J.-H. Choi, J.-M. Suh, I.-Y. Chang, D.-W. Shun, C.-K. Yi, J.-E. Son, S.-D. Kim, The effect of fine particles on elutriation of coarse particles in a gas fluidized bed, Powder Technol. 121 (2-3) (2001) 190–194.

[39] X. Ma, K. Kato, Effect of interparticle adhesion forces on elutriation of fine powders from a fluidized bed of a binary particle mixture, Powder Technol. 95 (2) (1998) 93–101.

[40] K. Smolders, J. Baeyens, Elutriation of fines from gas fluidized beds: mechanisms of elutriation and effect of freeboard geometry, Powder Technol. 92 (1997) 35–46.

[41] Y.-D. Liu, S. Kimura, Fluidization and entrainment of difficult-to-fluidize fine powder mixed with easy-to-fluidize large particles, Powder Technol. 75 (2) (1993) 189–196.

[42] J.M. Rodríguez, J.R. Sánchez, A. Alvaro, D.F. Florea, A.M. Estévez, Fluidization and elutriation of iron oxide particles, A study of attrition and agglomeration processes in fluidized beds, Powder Technol. 111 (3) (2000) 218–230.

[43] Y.-M. Chang, C.-M. Chou, K.-T. Su, C.-Y. Hung, C.-H. Wu, Elutriation characteristics of fine particles from bubbling fluidized bed incineration for sludge cake treatment, Waste Manage. 25 (3) (2005) 249–263.

[44] J. Li, T. Nakazato, K. Kato, Effect of cohesive powders on the elutriation of particles from a fluid bed, Chem. Eng. Sci. 59 (13) (2004) 2777–2782.

[45] S. Maurer, S.R. Durán, M. Künstle, S.M.A. Biollaz, Influence of interparticle forces on attrition and elutriation in bubbling fluidized beds, Powder Technol. 291 (2016) 473–486.

[46] S. Wang, B. Hu, S. Liu, W. Yin, K. Zhang, Investigation into the elutriation of fines from binary mixtures via CFD simulation with a multi-scale drag model, Powder Technol. 339 (2018) 633–640.

[47] M. Sciazko, J. Bandrowski, J. Raczek, On the entrainment of solid particles from a fluidized bed, Powder Technol. 66 (1) (1991) 33–39.

[48] E.R. Monazam, R.W. Breault, J. Weber, K.y. Layfield, Elutriation of fines from binary particle mixtures in bubbling fluidized bed cold model, Powder Technol. 305 (2017) 340–346.

[49] E. Kewes, F. Dahlem, S. Bec, N. Estime, E. Risse, J. Grollemund, J.-L. Loubet, The sequential elutriation behavior of wide particle size distributions, Powder Technol. 286 (2015) 230–239.

[50] J.A. Quevedo, R. Pfeffer, In Situ Measurements of Gas Fluidized Nanoagglomerates, Ind. Eng. Chem. Res. 49 (11) (2010) 5263–5269.

[51] D. Geldart, A.C.Y. Wong, Entrainment of particles from fluidized beds of fine powders, AIChE Symp. Ser. 83 (1987).

[52] L. Lin, J.T. Sears, C.Y. Wen, Elutriation and Attrition of Char from a Large Fluidized Bed, Powder Technol. 27 (1980) 105–115.

[53] L. de Martín, J. Sánchez-Prieto, F. Hernández-Jiménez, J.R. van Ommen, A settling tube to determine the terminal velocity and size distribution of fluidized nanoparticle agglomerates, J. Nanopart. Res. 16 (1) (2014), https://doi.org/10.1007/s11051-013-2183-3.